Inorganic Chemistry
Article

*Inorg. Chem.* **2010**, *49*, 7773–7782 **7773**
DOI: 10.1021/ic1005715

# Density Functional Theory Study on the Mechanism of the Reductive Cleavage of $CO_2$ by a Bis-$\beta$-Diketoiminatediiron Dinitrogen Complex

**Alireza Ariafard,*[,†,‡] Nigel J. Brookes,[‡] Robert Stranger,[§] Peter D.W. Boyd,[‡,∥] and Brian F. Yates*[,‡]**

[†]*Department of Chemistry, Faculty of Science, Central Tehran Branch, Islamic Azad University, Shahrak Gharb, Tehran, Iran,* [‡]*School of Chemistry, University of Tasmania, Private Bag 75, Hobart TAS 7001, Australia,* [§]*School of Chemistry, Australian National University, Canberra ACT 0200, Australia, and* [∥]*Department of Chemistry, The University of Auckland, Private Bag 92019, Auckland 1142, New Zealand*

Received March 26, 2010

Density functional theory has been used to analyze the detailed reaction mechanism for the reductive cleavage of $CO_2$ by a dinitrogen bridged bis-$\beta$-diketoiminatediiron complex, $L^{tBu}Fe-N_2-FeL^{tBu}$ (**I**), recently reported by Holland and co-workers. A number of pathways have been investigated and the most likely mechanism correlates well with experimental evidence. A rationale has been provided for the binding of $CO_2$, the release of CO, and the ready formation of $CO_3^{2-}$. Our results show that the insertion of $CO_2$ into the diiron complex is the rate determining step of the reductive cleavage reaction. An intramolecular reduction step from the reduced dinitrogen bridge is proposed which serves to increase the activation of $CO_2$. This is followed by an intersystem crossing from the septet to the nonet state which acts as a driving force for the subsequent release of CO. The overall reductive cleavage reaction is exergonic by 120 kJ/mol, and further reaction of the released CO with the starting diiron complex is also predicted to be strongly exergonic.

## Introduction

An increase in atmospheric $CO_2$ concentration is broadly responsible for the issue of global warming.[1] A conceivable approach for solving the problem is to use $CO_2$ as a precursor to the synthesis of high value products.[2] The transition metal-promoted coupling reaction between $CO_2$ and an unsaturated group, leading to the formation of a new covalent bond, has been introduced as a major step in $CO_2$ activation.[3,4] The reductive C−O scission of $CO_2$ using transition metal complexes is an alternative way for reducing the $CO_2$ concentration.[5] In this regard, Caulton and co-workers in a combined theoretical and experimental study, showed that [($^tBu_2PCH_2SiMe_2)_2N$]Ni is capable of breaking one of the C−O bonds of $CO_2$.[6] The reduction of $CO_2$ using [$PhBP^{CH_2Cy_3}$]Fe, where [$PhBP^{CH_2Cy_3}$] = [$PhB(CH_2P(CH_2Cy)_2)_3$]$^-$, was also reported by Peters et al.[7] Sadighi and co-workers also showed that a (NHC)Ni complex (NHC = N-heterocyclic carbene) is capable of promoting the reductive disproportionation reaction $2CO_2 + 2e^- \rightarrow CO + CO_3^{2-}$.[8] Theoretical studies carried out by Li and Lin established that transfer of an oxygen atom from a side-on bonded $CO_2$ ligand to an incoming $CO_2$ results

*To whom correspondence should be addressed. E-mail: ariafard@yahoo.com (A.A.); brian.yates@utas.edu.au (B.F.Y.).

(1) (a) Hoffert, M. I. *Science* **2002**, *298*, 981. (b) Lackner, K. S. *Science* **2003**, *300*, 1677. (c) Pacala, S.; Socolow, R. *Science* **2004**, *305*, 968. (d) Thomas, C. D.; Cameron, A.; Green, R. E.; Bakkenes, M.; Beaumont, L. J.; Collingham, Y. C.; Erasmus, B. F. N.; de Siqueira, M. F.; Grainger, A.; Hannah, L.; Hughes, L.; Huntley, B.; van Jaarsveld, A. S.; Midgley, G. F.; Miles, L.; Ortega-Huerta, M. A.; Peterson, A. T.; Phillips, O. L.; Williams, S. E. *Nature* **2004**, *427*, 145. (e) Bauen, A. *J. Power Sources* **2006**, *157*, 893.

(2) (a) Chan, B.; Radom, L. *J. Am. Chem. Soc.* **2006**, *128*, 5322. (b) Chan, B.; Radom, L. *J. Am. Chem. Soc.* **2008**, *130*, 9790.

(3) (a) Pellny, P.-M.; Kirchbauer, F. G.; Vladimir, V. B.; Baumann, W.; Spannenberg, A.; Rosenthal, U. *J. Am. Chem. Soc.* **1999**, *121*, 8313. (b) Arakawa, H.; Aresta, M.; Armor, J. N.; Barteau, M. A.; Beckman, E. J.; Bell, A. T.; Bercaw, J. E.; Creutz, C.; Dinjus, E.; Dixon, D. A.; Domen, K.; DuBois, D. L.; Eckert, J.; Fujita, E.; Gibson, D. H.; Goddard, W. A.; Goodman, D. W.; Keller, J.; Kubas, G. J.; Kung, H. H.; Lyons, J. E.; Manzer, L. E.; Marks, T. J.; Morokuma, K.; Nicholas, K. M.; Periana, R.; Que, L.; Rostrup-Nielson, J.; Sachtler, W. M. H.; Schmidt, L. D.; Sen, A.; Somorjai, G. A.; Stair, P. C.; Stults, B. R.; Tumas, W. *Chem. Rev.* **2001**, *101*, 953. (c) Gibson, D. H. *Chem. Rev.* **1996**, *96*, 2063. (d) Gibson, D. H. *Coord. Chem. Rev.* **1999**, *186*, 335. (e) Knobloch, D. J.; Toomey, H. E.; Chirik, P. J. *J. Am. Chem. Soc.* **2008**, *130*, 4248. (f) Louie, J.; Gibby, J. E.; Farnworth, M. V.; Tekave, T. N. *J. Am. Chem. Soc.* **2002**, *124*, 15188. (g) Jeske, R. C.; Rowley, J. M.; Coates, G. W. *Angew. Chem., Int. Ed.* **2008**, *47*, 6041. (h) Cohen, C. T.; Chu, T.; Coates, G. W. *J. Am. Chem. Soc.* **2005**, *127*, 10869. (i) Bhattacharyya, K. X.; Akana, J. A.; Laitar, D. S.; Berlin, J. M.; Sadighi, J. P. *Organometallics* **2008**, *27*, 2682.

(4) For theoretical studies see: (a) Ohnishi, Y.-y.; Matsunaga, T.; Nakao, Y.; Sato, H.; Sakaki, S. *J. Am. Chem. Soc.* **2005**, *127*, 4021. (b) Graham, D. C.; Mitchell, C.; Bruce, M. I.; Metha, G. F.; Bowie, J. H.; Buntine, M. A. *Organometallics* **2007**, *26*, 6784. (c) Graham, D. C.; Bruce, M. I.; Metha, G. F.; Bowie, J. H.; Buntine, M. A. *J. Organomet. Chem.* **2008**, *693*, 2703. (d) Li, J.; Jia, G.; Lin, Z. *Organometallics* **2008**, *27*, 3892.

(5) (a) Procopio, L. J.; Carroll, P. J.; Berry, D. H. *Organometallics* **1993**, *12*, 3087. (b) Laitar, D. S.; Müller, P.; Sadighi, J. P. *J. Am. Chem. Soc.* **2005**, *127*, 17196. (c) Zhao, H.; Lin, Z.; Marder, T. B. *J. Am. Chem. Soc.* **2006**, *128*, 15637. (d) Allen, O. R.; Dalgarno, S. J.; Field, L. D. *Organometallics* **2008**, *27*, 3328.

(6) Fullmer, B. C.; Fan, H.; Pink, M.; Caulton, K. E. *Inorg. Chem.* **2008**, *47*, 1865.

(7) Lu, C. C.; Saouma, C. T.; Day, M. W.; Peters, J. C. *J. Am. Chem. Soc.* **2007**, *129*, 4.

(8) Lee, C. H.; Laitar, D. S.; Mueller, P.; Sadighi, J. P. *J. Am. Chem. Soc.* **2007**, *129*, 13802.


Published on Web 08/11/2010

in breaking of the C−O bond of the bound $CO_2$ and formation of $CO_3^{2-}$.[9] In a DFT study, we also rationalized why the Laplaza/Cummins $L_3Mo$ (L = N(R)Ar) system[10] with a $d^3$ configuration is unreactive toward the reduction of $CO_2$ to give $L_3Mo{=}O + L_3Mo{-}CO$, and why the $d^2$ 3-coordinate systems such as $L_3Nb$ and $L_3Ta$ are reactive.[11] The mechanism of the reaction of (NHC)CuBpin + $CO_2$ → (NHC)CuOBpin + CO (pin = pinacolate = $OCMe_2CMe_2O$)[5b] was revealed by Lin and co-workers.[5c] They showed that the boryl group migrates to the carbon atom of $CO_2$ followed by the CO elimination through the subsequent migration of the boryl group from carbon to oxygen to form (NHC)CuOBpin + CO.

$$1.25\ \underset{\mathbf{I}}{L^{tBu}Fe\text{-}N_2\text{-}FeL^{tBu}} + 2\ CO_2 \rightarrow 0.5\ \underset{\mathbf{II}}{L^{tBu}Fe(CO)_2} + \underset{\mathbf{III}}{L^{tBu}Fe\text{-}CO_3\text{-}FeL^{tBu}} + 1.25\ N_2 \quad (1)$$

**Scheme 1**

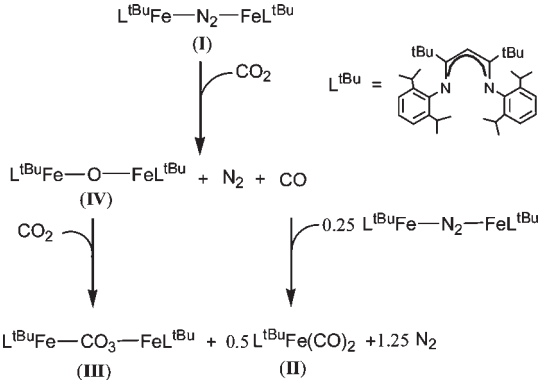


An interesting example of these processes is the cleavage of $CO_2$ by the diiron(I) complex $L^{tBu}Fe{-}N_2{-}FeL^{tBu}$ (**I**), where $L^{tBu}$ = 2,2,6,6-tetramethyl-3,5-bis[(2,6-diisopropylphenyl)-imino]hept-4-yl,[12] affording a mixture of the dicarbonyliron(I) complex $L^{tBu}Fe(CO)_2$ (**II**) and the carbonatodiiron(II) complex $L^{tBu}Fe{-}CO_3{-}FeL^{tBu}$ (**III**) (see eq 1).[13] The mechanism shown in Scheme 1 was proposed for this reaction (the reductive C−O scission of $CO_2$ using **I**). It includes the following steps: (1) The formation of the oxodiiron(II) complex $L^{tBu}Fe{-}O{-}FeL^{tBu}$ (**IV**) through the treatment of the septet complex **I** with $CO_2$. It is at this stage that the reductive scission of the C═O bond is proposed to occur. (2) The $L^{tBu}Fe{-}CO_3{-}FeL^{tBu}$ complex **III** is formed via the reaction of $CO_2$ with $L^{tBu}Fe{-}O{-}FeL^{tBu}$. (3) The CO molecule released from stage 1 then interacts with **I** to afford **II**. In this study, we investigate the proposed mechanism in more detail using density functional theory (DFT). We hope that the current study provides insight into how and why the diiron(I) complex is reactive toward the reduction of $CO_2$. This paper also discusses how the shift between different spin states on the potential energy surface affects the reaction mechanism of the $CO_2$ cleavage. In this report, we also try to understand why $L^{tBu}Fe{-}O{-}FeL^{tBu}$ has a strong tendency to react with $CO_2$.[13] To date, all the theoretical studies have focused only on the structure and bonding of such Fe complexes.[12,14] An understanding of the reaction mechanism will be helpful in the design of new Fe reactants for the breaking of small molecules.

## Computational Details

Gaussian 03[15] was used to fully optimize all the structures reported in this paper at the B3LYP level of DFT.[16] The effective core potential of Hay and Wadt with a double-ζ valence basis set (LANL2DZ) was chosen to describe Fe.[17] The 6-31G(d) basis set was used for other atoms.[18] This basis set combination will be referred to as BS1. Frequency calculations were carried out at the same level of theory as for structural optimization. To further refine the energies obtained from the B3LYP/BS1 calculations, we carried out single point energy calculations for all the structures with a larger basis set (BS2). BS2 comprises the 6-311+G(3df) basis set for Fe and the 6-311+G(2d,p) basis set for the other atoms. Comparisons of single point energies using the B3PW91 functional[19] have also been carried out and are available in Supporting Information. This functional does not alter the overall outcome of the B3LYP potential energy surface and reconfirms the insertion reaction of $CO_2$ between the two Fe atoms as the rate determining step. To estimate the corresponding Gibbs free energies, the entropy corrections were calculated at the B3LYP/BS1 level and added to all the single point energy calculations.

We have used the B3LYP/BS2//B3LYP/BS1 energies throughout the paper unless otherwise stated. The high spin multiplicity encountered resulted in the use of the computationally expensive quadratic convergence routine (scf = qc) for most of the geometry optimizations.[20] Full molecular optimization would thus be computationally expensive and hence a reduced model has been employed (vide infra). The NBO program, as implemented in Gaussian 03, was used to analyze the natural bond orbitals and the second order interaction energies for some of the species involved in the reaction.[21]

(9) Li, J.; Lin, Z. *Organometallics* **2009**, *28*, 4231.
(10) Johnson, A. R.; Davis, W. M.; Cummins, C. C.; Serron, S.; Nolan, S. P.; Musaev, D. G.; Morokuma, K. *J. Am. Chem. Soc.* **1998**, *120*, 2071.
(11) Brookes, N. J.; Ariafard, A.; Stranger, R.; Yates, B. F. *Dalton Trans.* **2009**, 9266.
(12) (a) Smith, J. M.; Lachicotte, R. J.; Pittard, K. A.; Cundari, T. R.; Lukat-Rodgers, G.; Rodgers, K. R.; Holland, P. L. *J. Am. Chem. Soc.* **2001**, *123*, 9222. (b) Smith, J. M.; Sadique, A. R.; Cundari, T. R.; Rodgers, K. R.; Lukat-Rodgers, G.; Lachicotte, R. J.; Flaschenriem, C. J.; Vela, J.; Holland, P. L. *J. Am. Chem. Soc.* **2006**, *128*, 756. (c) Stoian, S. A.; Vela, J.; Smith, J. M.; Sadique, A. R.; Holland, P. L.; Münck, E.; Bominaar, E. L. *J. Am. Chem. Soc.* **2006**, *128*, 10181. (d) Holland, P. L. *Acc. Chem. Res.* **2008**, *41*, 905.
(13) Holland and coworkers showed that the diiron(I) complex $L^{tBu}Fe{-}N_2{-}FeL^{tBu}$ (**I**) reacts with 2 equiv of dry $CO_2$ at room temperature and gives directly a mixture of $L^{tBu}Fe(CO)_2$ and $L^{tBu}Fe{-}CO_3{-}FeL^{tBu}$ without observation of any stable intermediates. They also reported that $L^{tBu}Fe{-}O{-}FeL^{tBu}$ at room temperature is active towards reaction with $CO_2$ to afford $L^{tBu}Fe{-}CO_3{-}FeL^{tBu}$; Sadique, A. R.; Brennessel, W. W.; Holland, P. L. *Inorg. Chem.* **2008**, *47*, 784.
(14) Yu, Y.; Sadique, A. R.; Smith, J. M.; Dugan, T. R.; Cowley, R. E.; Brennessel, W. W.; Flaschenriem, C. J.; Bill, E.; Cundari, T. R.; Holland, P. L. *J. Am. Chem. Soc.* **2008**, *130*, 6624.
(15) Frisch, M. J.; et al. *Gaussian 03*, revision B.05; Gaussian, Inc.: Pittsburgh, PA, 2003.
(16) (a) Lee, C. T.; Yang, W. T.; Parr, R. G. *Phys. Rev. B* **1988**, *37*, 785. (b) Miehlich, B.; Savin, A.; Stoll, H.; Preuss, H. *Chem. Phys. Lett.* **1989**, *157*, 200. (c) Becke, A. D. *J. Chem. Phys.* **1993**, *98*, 5648.
(17) (a) Hay, P. J.; Wadt, W. R. *J. Chem. Phys.* **1985**, *82*, 270. (b) Wadt, W. R.; Hay, P. J. *J. Chem. Phys.* **1985**, *82*, 284.
(18) Hariharan, P. C.; Pople, J. A. *Theor. Chim. Acta* **1973**, *28*, 213.
(19) (a) Becke, A. D. *Phys. Rev. A* **1988**, *38*, 3098. (b) Burke, K.; Perdew, J. P.; Wang, Y.; Dobson, J. F.; Vignale, G.; Das, M. P. *Electronic Density Functional Theory: Recent Progress and New Directions*; Plenum: New York, 1998. (c) Perdew, J. P.; Chevary, J. A.; Vosko, S. H.; Jackson, K. A.; Pederson, M. R.; Singh, D. J.; Fiolhais, C. *Phys. Rev. B* **1992**, 46. (d) Perdew, J. P.; Chevary, J. A.; Vosko, S. H.; Jackson, K. A.; Pederson, M. R. D.; Singh, J.; Fiolhais, C. *Phys. Rev. B* **1993**, 48. (e) Perdew, J. P.; Burke, K.; Wang, Y. *Phys. Rev. B* **1996**, *54*, 16533.
(20) Bacskay, G. B. *Chem. Phys.* **1981**, *61*, 385.
(21) Glendening, E. D.; Read, A. E.; Carpenter, J. E.; Weinhold, F. *NBO*, version 3.1; Gaussian, Inc.: Pittsburgh, PA, 2003.

Minimum energy crossing points (MECPs) between states in the septet and nonet reaction paths have been located using either the code of Harvey et al. at the B3LYP/BS1 level of theory[22] or with the program ORCA[23] using the B3LYP functional with a 6-31G(d)[C,H, N, O], TZP[Fe], BS3, basis. Both of these models give similar crossing point energies relative to the higher lying septet state. Exchange coupling constants between the iron atoms for the intermediates in the concerted reaction were calculated using the broken symmetry approach of Noodleman.[23b] This involves DFT calculations for the low spin open-shell molecules in which the $\alpha$ and $\beta$ densities are allowed to localize on different atomic centers. The procedure used was that implemented by Neese in the program ORCA using the B3LYP/BS3 model.[23c]

## Results and Discussion

As stated in the Introduction, we shall here investigate the mechanism formulated by Holland and co-workers (Scheme 1) to show how $L^{tBu}Fe-N_2-FeL^{tBu}$ is capable of

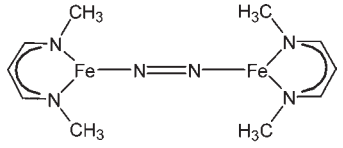

**1**

breaking the C=O bond of $CO_2$. For this purpose, we used the model reactant complex **1** in which the Ar substituents at N and the *tert*-butyl groups in $L^{tBu}Fe-N_2-FeL^{tBu}$ were substituted by $CH_3$ and H, respectively. In previous work on other transition metal systems, it has been shown that the replacement of Ar substituents at N by Me groups reproduces much better the experimental results than replacement by H atoms.[24] The overall energy profile for the reaction of **1** with $CO_2$ affording $LFe-CO_3-FeL$ is plotted in Figure 1 (insertion of $CO_2$) and Figure 3 (reductive cleavage of $CO_2$). It follows from this profile that, in good agreement with the experimental findings, $LFe-N_2-FeL$ is capable of breaking a C=O bond of $CO_2$. **N_X** and **NTS_X** in the figures are the nomenclatures used for the species on the relative energy surface, where **X** = **Du** stands for doublet, **Qa** for quartet, **Sp** for septet, and **Nn** for nonet spin states. **N** represents the minimum structures, and **NTS** corresponds to the transition structures on the B3LYP relative energy surface. Throughout the paper, the relative free energies calculated at 298.15 K and 1 atm are used to analyze the reaction mechanism while the corresponding electronic energies are given in parentheses for comparison. While being aware that the $\Delta G$ values are overestimated from the gas phase calculations because of the suppression of the rotational and translational motions in solution, we will see in the discussion that the errors in $\Delta G$ do not change the conclusions made here.

**1. Reductive C−O Cleavage of $CO_2$ and Formation of LFeOFeL.** Different possibilities for the mechanism of the $CO_2$ cleavage and the formation of the LFeOFeL complex were explored with the DFT calculations, and the results of the calculations are shown in Figures 1 and 3. The optimized geometries of the selected stationary points involved in these mechanisms are shown in Figure 2. In all cases the initial electronic state of the reactants is an overall septet state ($LFe-N_2-FeL$) and the final state of the products is a nonet state ($LFe(CO_3)FeL$). This implies that at some point in the reaction path there will

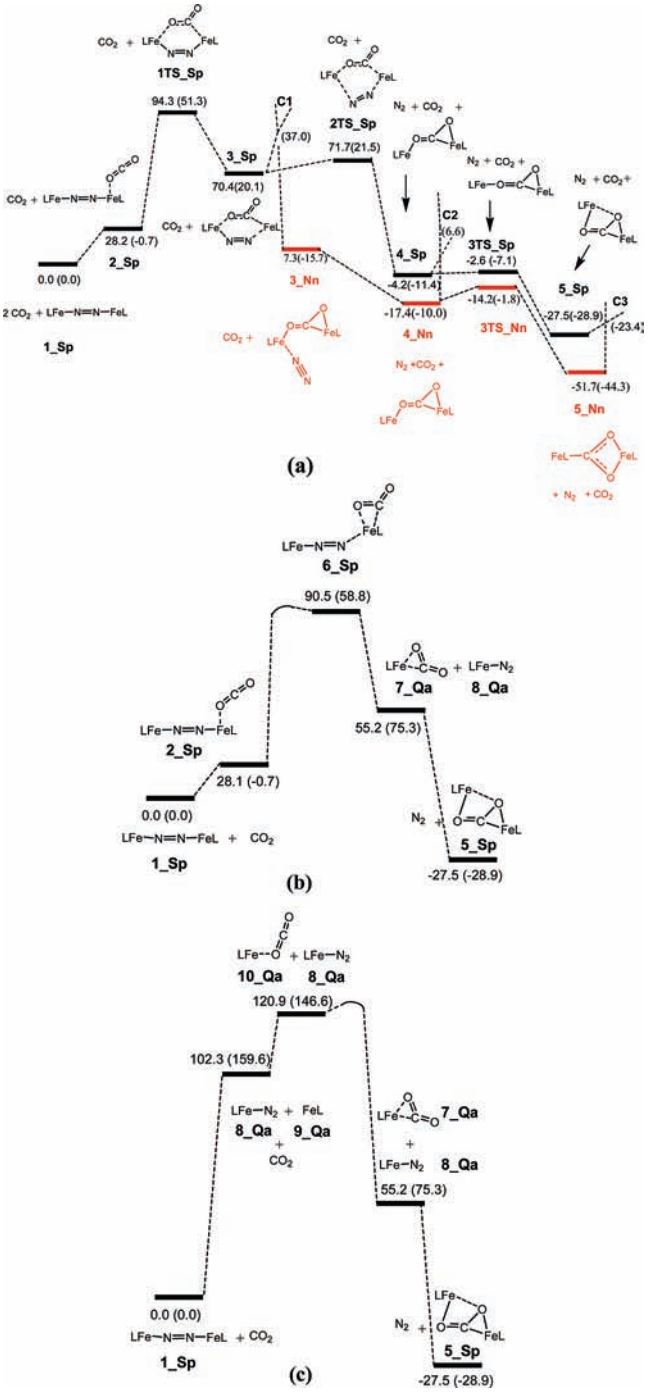


**Figure 1.** Energy profiles calculated for the $CO_2$ insertion into Fe···Fe through three different pathways: (a) concerted, (b) stepwise, and (c) dissociative. The relative free energies and electronic energies (in parentheses) obtained from the B3LYP/BS2//B3LYP/BS1 calculations are given in kJ/mol.

(22) (a) Harvey, J. N.; Aschi, M.; Schwarz, H.; Koch, W. *Theor. Chem. Acc.* **1998**, *99*, 95. (b) Harvey, J. N.; Aschi, M. *Phys. Chem. Chem. Phys.* **1999**, *1*, 5555.

(23) (a) Neese, F. *ORCA − an ab initio, Density Functional and Semi-empirical program package*, Version 2.7; University of Bonn: Bonn, Germany, 2009. (b) Noodleman, L. *J. Chem. Phys.* **1981**, *74*, 5737. (c) Neese, F. *J. Phys. Chem. Solids* **2004**, *65*, 781.

(24) Ariafard, A.; Lin, Z.; Jordan, R. F. *Organometallics* **2005**, *24*, 5140.

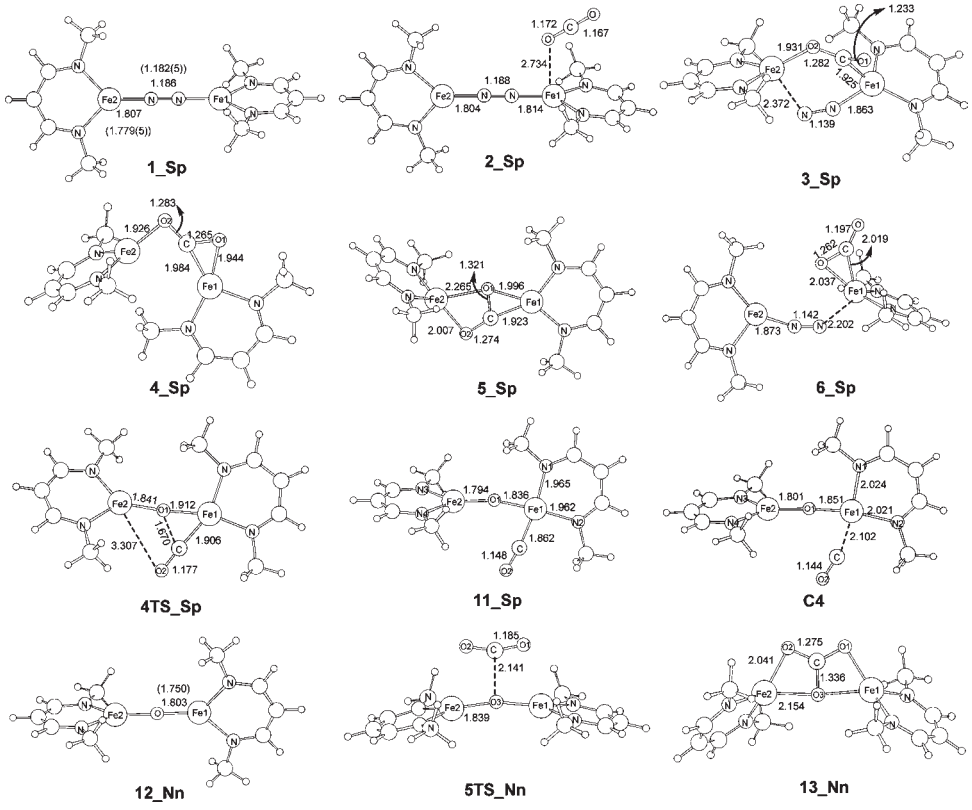


**Figure 2.** Optimized structures with selected structural parameters (bond length in Å) for some of the species involved in the energy profiles shown in Figures 1 and 3. Experimental X-ray structure values are shown in parentheses for **1_Sp**.

be a crossing from the septet to the nonet state. We have found several possible points in the reaction path where this may occur and have characterized these points using MECP calculations. It should also be noted that the spin states of the bimetallic species assume only weak interactions between the paramagnetic ions. This has been explored using broken symmetry calculations.

**1.1. Insertion of $CO_2$ into Fe−$N_2$−Fe Complex I.** The first step of the reaction is surmised to be the insertion of $CO_2$ into the LFe−$N_2$−FeL complex. Three different pathways for the $CO_2$ insertion were considered: concerted, stepwise, and dissociative. In the concerted pathway, $CO_2$ simultaneously interacts with both the Fe metal centers and gives the dinuclear intermediate $LFeCO_2FeL$. In the stepwise pathway, $CO_2$ interacts with one of the Fe centers of **1_Sp** in an $\eta^2$-side-on coordination mode, weakening the ($\eta^2$-$CO_2$)Fe−$N_2$ bond. The complex L($\eta^2$-$CO_2$)Fe−$N_2$−FeL then dissociates to LFe($\eta^2$-$CO_2$) and $LFeN_2$ followed by the coordination of the $CO_2$ ligand of LFe($\eta^2$-$CO_2$) to the metal center of $LFeN_2$ to afford $LFeCO_2FeL$. The dissociative pathway starts with the dissociation of LFe from LFe−$N_2$−FeL, is followed by the coordination of $CO_2$ to LFe in an $\eta^2$-side-on fashion, and finally the LFe($\eta^2$-$CO_2$) interacts with $LFeN_2$ to give $LFeCO_2FeL$. Here, we will study all the pathways in detail.

**1.1.1. Concerted Pathway.** The first step in this pathway is the binding of $CO_2$ to **1_Sp** (Figure 1a). The ground state for **1** is a septet, a result which is in a good agreement with earlier experimental and theoretical evidence (the previous theoretical study employed a simpler version of **1** in which the $CH_3$ groups were replaced by H).[12] The X-ray crystal structure for $L^{tBu}Fe-N_2-FeL^{tBu}$ was reasonably reproduced using the B3LYP/BS1 calculations on the model complex **1_Sp** (see Figure 2). The calculated dihedral angle between two Fe-ketiminate moieties of **1_Sp** is about 99.8°. Consideration of the Mulliken charges and spin populations indicate that the electronic state in **1** is best described as resulting from a strong antiferromagnetic interaction between two high-spin Fe(II) ions and a triplet state $N_2^{2-}$ anion.[12c] A broken symmetry calculation for this configuration gave an exchange coupling constant ($-2JS_1 \cdot S_2$) $J = -1303$ $cm^{-1}$ in comparison to estimates for the coplanar $D_{2h}$ symmetry complex $J = -1809$ $cm^{-1}$.[12c] Attempts to obtain the coplanar form of **1_Sp** led to a structure with a dihedral angle of 37.0° lying 3.8 kJ/mol above **1_Sp**.

In the initial encounter $CO_2$ approaches one of the Fe metal centers of **1_Sp** via an $\eta^1$-end-on mode,[25] giving the weakly bound complex **2_Sp** in which the initial **1_Sp** moiety is only weakly perturbed. From **2_Sp**, $CO_2$ can directly insert between the Fe atoms to generate **3_Sp** via the transition structure **1TS_Sp** with a calculated barrier of 94.3 kJ/mol, Figure 1a. **3_Sp** is higher in energy than **1_Sp** + $CO_2$ by 70.4 kJ/mol. In **1TS_Sp** there is a partial shift of charge and spin from the bridging $N_2^{2-}$ to the bridging $CO_2$, a process that is near completion in **3_Sp**. The Mulliken electron population of $CO_2$ changes from +0.064 in **2_Sp** to −0.084 in **1TS_Sp** to −0.484 in **3_Sp**. There is a corresponding lengthening of the

(25) Attempts to calculate an intermediate in which $CO_2$ coordinates to a Fe metal center via its carbon center result in the formation of intermediate **6_SP** (Figure 1b).

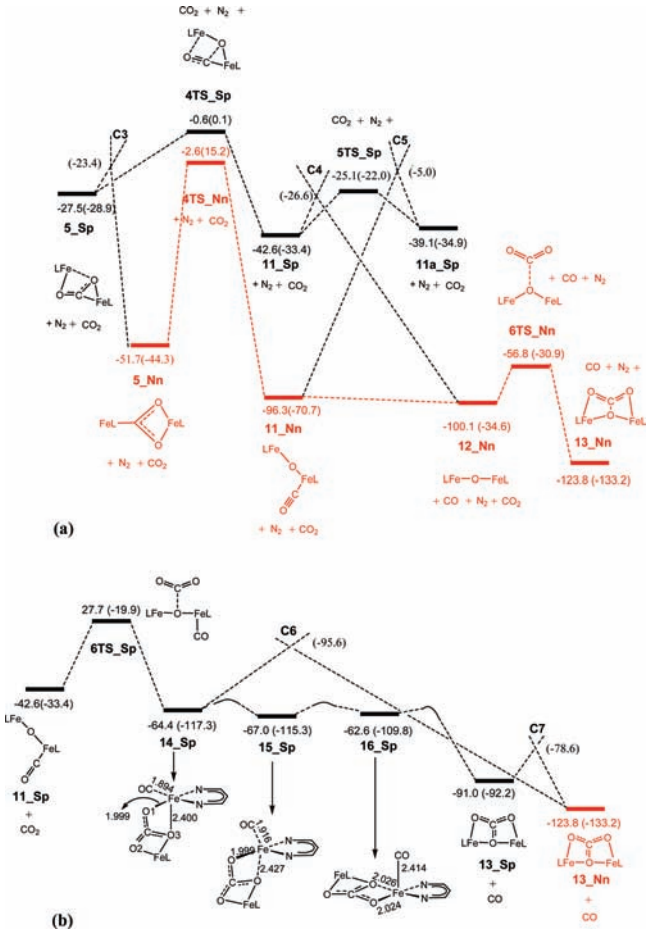


**Figure 3.** (a) Energy profile calculated for the $CO_2$ cleavage reaction and the reaction of LFe−O−FeL with $CO_2$ for the formation of $LFeCO_3FeL$. (b) Two alternative pathways for the formation of $LFeCO_3FeL$ from the reaction of LFe−O−Fe(CO)L with $CO_2$. The relative free energies and electronic energies (in parentheses) obtained from the B3LYP/BS2//B3LYP/BS1 calculations are given in kJ/mol.

C−O distances and a bending of the $CO_2$ moiety in **3_Sp** (see Figure 2). The insertion of the $\pi$-acid $CO_2$ molecule reduces the Fe-to-$N_2$ charge transfer, as evidenced by the less negative charge of −0.210 on $N_2$ in **3_Sp** versus −0.474 in **1TS_Sp** versus −0.548 in **1_Sp**. The $CO_2$ insertion also weakens the Fe−$N_2$−Fe bonds; the Fe1−N1 and Fe2−N2 bonds in **3_Sp** are lengthened by 0.048 and 0.568 Å, respectively, as compared to their corresponding Fe−N bonds in **2_Sp** (see Figure 2). Indeed, the inserted $CO_2$ ligand competes against the $N_2$ ligand for back-donation, weakening the Fe−$N_2$−Fe bonds.

Two pathways are then possible: First $N_2$ dissociation from **3_Sp** to generate **4_Sp** could occur through the low energy transition structure **2TS_Sp** which lies only 1.3 kJ/mol uphill of **3_Sp**. The free energy change for the $N_2$ dissociation is −67.8 kJ/mol. Thus, the dissociation process is both kinetically and thermodynamically possible. The $N_2$ dissociation, leading to an increase in $CO_2$ activation, enhances the stability of the coordination complex **4_Sp** relative to **3_Sp**; the charge carried by $CO_2$ in **4_Sp** (−0.583) is more negative than in **3_Sp** (−0.484). In other words, the stronger Fe−$CO_2$−Fe bonding interactions in **4_Sp** counteract the energy needed for breaking of the Fe−$N_2$−Fe bonds. The $N_2$ binding free energies in LFe−$N_2$−FeL (eq 2) and LFe−$N_2$ (eq 3) are calculated as 102.3 and 51.3 kJ/mol, respectively.

$$\underset{\text{(septet)}}{\text{LFe}-\text{N}{=}\text{N}-\text{FeL}} \xrightarrow[102.3\ \text{kJ/mol}]{\Delta E1=} \underset{\text{(quartet)}}{\text{LFe}-\text{N}\equiv\text{N}} + \underset{\text{(quartet)}}{\text{LFe}} \qquad (2)$$

$$\underset{\text{(quartet)}}{\text{LFe}-\text{N}\equiv\text{N}} \xrightarrow[51.3\ \text{kJ/mol}]{\Delta E2=} \underset{\text{(singlet)}}{\text{N}\equiv\text{N}} + \underset{\text{(quartet)}}{\text{LFe}} \qquad (3)$$

An alternative pathway involves an intersystem crossing from **3_Sp** to a nonet state complex **3_Nn**. The MECP **C1**, at the B3LYP/BS3 level of theory was found to be about 16.9 kJ/mol above the energy of **3_Sp** (Figure 1a). The resultant lower energy nonet state complex **3_Nn** is weakly stable with nitrogen bound to a single iron atom. Nitrogen dissociates in a near barrierless process to give the $CO_2$ bridged complex **4_Nn**.

In **4_Sp**, $CO_2$ is bound to Fe2 through one of the oxygen atoms of $CO_2$. A structural rearrangement through the transition structure **3TS_Sp** (Figure 1a), with a small barrier of 1.6 kJ/mol, gives the $\eta^2$-end-on coordination complex **5_Sp** in which both of the oxygen atoms of $CO_2$ coordinate with Fe2 (Figure 2). $CO_2$ in **5_Sp** is more activated than in **4_Sp**, as judged from the more negative charge carried by $CO_2$ (−0.665) as well as the longer C−O bond distances in **5_Sp**. The increased level of the $CO_2$ activation in **5_Sp** is reflected in the greater stability of **5_Sp** versus **4_Sp**.

On the nonet surface, **4_Nn**, which arises from **3_Nn**, may also occur by an intersystem crossing from **3_Sp**. The MECP, **C2**, for this second process occurs 18 kJ/mol in energy above **3_Sp**. **4_Nn** rearranges via a low energy (3.2 kJ/mol) transition structure **3TS_Nn** to give the equivalent complex **5_Nn**. Again this species is lower in energy (by 24.2 kJ/mol) than **5_Sp** on the septet surface. A MECP, **C3**, between **5_Sp** and **5_Nn** has been calculated to be only 5.5 kJ/mol above the **5_Sp** ground state. The $CO_2$ molecule bound in **5_Nn** is similar to that found in **5_Sp**. The $CO_2$ is again more activated than in initially formed **4_Nn** with more negative charge (−0.688 **4_Nn** vs −0.767 **5_Nn**) and again longer C−O bond distances. The preference for the isomer **5_Sp** over **4_Sp** and **5_Nn** over **4_Nn** is also supported by experimental geometries for other mixed metal systems M/$CO_2$/M′.[26] Our calculations predict a distorted tetrahedral coordination around Fe2 in **5_Sp** (the Fe2−O1 distance is 0.257 Å longer than the Fe2−O2 distance) while in **5_Nn** the coordination geometry is more regular with Fe−O bond distances of 2.129 and 2.072 Å .

**1.1.2. Stepwise Pathway.** This pathway starts with the interconversion of the $\eta^1$-end-on coordination mode of $CO_2$ to $\eta^2$-side-on mode, leading to the formation of **6_Sp** (Figure 1b). Because of the flatness of the relative energy surface in the vicinity of the intermediate **6_Sp**, no transition state is located for the conversion of **2_Sp** → **6_Sp**. **6_Sp** is much less stable than **2_Sp** indicating that the Fe1 atom in **2_Sp** is very reluctant to coordinate $CO_2$ through the $\eta^2$-side-on mode. In other words, one metal center in LFe−$N_2$−FeL is not sufficiently electron-rich to yield a relatively stable $\eta^2$-side-on species. The coordination

(26) (a) Gibson, D. H.; Ye, M.; Richardson, J. F.; Mashuta, M. S. *Organometallics* **1994**, *13*, 4559. (b) Lutz, M.; Haukka, M.; Pakkanen, T. A.; Gade, L. H. *Organometallics* **2001**, *20*, 2631. (c) Gibson, D. H.; Sleadd, B. A.; Mashuta, M. S.; Richardson, J. F. *Organometallics* **1997**, *16*, 4421.

of $CO_2$ in side-on mode substantially reduces the Fe1-to-$N_2$ charge transfer and thus weakens the Fe1−$N_2$ bond; the negative charge on $N_2$ decreases from −0.578 in **2_Sp** to −0.204 in **6_Sp**, and the Fe1−$N_2$ bond lengthens from 1.807 Å in **2_Sp** to 2.202 Å in **6_Sp** (Figure 2). **6_Sp** easily dissociates into LFe($\eta^2$-$CO_2$) (**7_Qa**) and LFe$N_2$ (**8_Qa**) with a reaction free energy of −35.3 kJ/mol. At the end, the reaction of **7_Qa** with **8_Qa** leads to the $N_2$ loss and the formation of **5_Sp**.

**1.1.3. Dissociative Pathway.** In this pathway, the reaction proceeds first via breaking one of the Fe−$N_2$ bonds in **1_Sp** and subsequently furnishing LFe−$N_2$ and LFe (Figure 1c). This process is thermodynamically unfavorable and requires about 102.3 kJ/mol. The coordination of $CO_2$ to LFe via an $\eta^1$-end-on fashion then gives **10_Qa**, being thermodynamically 18.6 kJ/mol less stable than **1_Sp** + $CO_2$. After that, the $CO_2$ ligand in **10_Qa** undergoes a barrierless interconversion from $\eta^1$-end-on to $\eta^2$-side-on to generate **7_Qa**. Unlike in the case of LFe$N_2$-FeL, the $\eta^2$-side-on coordination of $CO_2$ to LFe is strongly preferred; **7_Qa** is 65.7 kJ/mol below **10_Qa**. This is logical because the absence of the $\pi$-acid $N_2$ ligand in the less saturated species LFe increases the capability of the Fe metal center to force $CO_2$ coordination via an $\eta^2$-side-on fashion.

Comparing the energy profiles shown in Figure 1, it appears that the concerted and stepwise pathways are the most accessible processes with lower lying barriers. However, on the basis of our calculations, distinguishing between these two pathways, concerted and stepwise, is difficult. This argument can be further supported by the B3PW91/BS2//B3LYP/BS1 calculations. Using the B3LYP functional, the energy maxima for the concerted, stepwise, and dissociative pathways are computed as 94.3 (51.3), 90.5 (58.8), and 120.9 (146.6) kJ/mol, respectively. Using the B3PW91 functional the energy maxima are 93.0 (50.0), 90.1 (58.1), and 132.8 (158.8) kJ/mol, respectively. This comparison also confirms that a little variation in $\Delta G^{\ddagger}$ and $\Delta E^{\ddagger}$ upon going from B3LYP to B3PW91 is observed.

**1.2. Breaking $CO_2$.** The complexes **5_Sp** and **5_Nn** can undergo a C−O cleavage reaction via the transition structures **4TS_Sp** or **4TS_Nn** to form **11_Sp** or **11_Nn** with two formal Fe(II) metal centers (Figure 3a), a bridging oxide anion, and a carbonyl ligand bound to an Fe(II) center. The reaction is a favorable process; **5_Sp** → **11_Sp** is about −15.1 kJ/mol exergonic and takes place through a transition structure (**4TS_Sp**) lying only 26.9 kJ/mol above **5_Sp**. In comparison the MECP **5_Sp** → **5_Nn** lies 5.5 kJ/mol above **5_Sp.** In the analogous nonet pathway **5_Nn** → **11_Nn** is about −44.6 kJ/mol exergonic and takes place through a transition structure (**4TS_Nn**) lying 49.1 kJ/mol above **5_Nn**. In **4TS_Sp**, Fe2 approaches closer to O1 with a Fe2−O1 distance of 1.841 Å, the Fe2−O2 bond is nearly broken, and the C−O1 bond is lengthened by 0.349 Å while in **4TS_Nn**, Fe2 approaches O1 with a Fe2−O1 distance of 1.887 Å, the Fe2−O2 bond is nearly broken, and the C−O1 bond is lengthened by about 0.463 Å . The calculations indicate that Fe1 in **11_Sp** adopts a square planar structure in which Fe1, CO, O1, and L are almost coplanar. From this result, one expects that the charge transfer leading to the reductive C−O cleavage of $CO_2$ should take place from the $d_{xy}$ orbital, being mainly localized on Fe1, to the

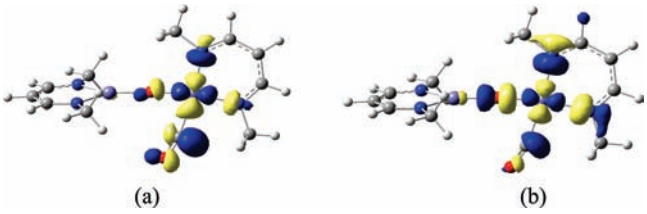


**Figure 4.** Spatial plots for (a) the LUMO of **C4** in the septet state and (b) the HOMO of **C4** in the nonet state.

$\sigma^*_{C-O1}$ orbital of $CO_2$. This interaction results in the full depopulation of the Fe1 $d_{xy}$ orbital and makes this orbital available for coordinating CO, giving **11_Sp** with a square planar geometry around Fe1. The Fe1−CO bond energy of 76.0 kJ/mol in **11_Sp** suggests that CO is strongly coordinated to Fe1 on the septet surface.

The structure **11_Nn**, with a nonet state arising from the **4TS_Nn** transition structure, is more stable than **11_Sp** (Figure 3a). This is in accord with the experimental evidence which reported high spin Fe(II) centers for compounds such as $L^{tBu}Fe-CO_3-FeL^{tBu}$ and $L^{tBu}Fe-O-FeL^{tBu}$.[13,27] The MECP, **C4**, has been located to be about 6.8 kJ/mol higher in energy than that of **11_Sp** (Figure 3a). Geometry optimization directly after the intersystem crossing along the nonet surface, or starting from the structure of **11_Sp** in the nonet state, spontaneously leads to the cleavage of the Fe−CO bond, forming the oxodiiron(II) complex LFe−O−FeL (**12_Nn**) as the product of the intersystem crossing process. The **11_Sp** → **12_Nn** + CO reaction is predicted to be feasible thermodynamically with a reaction free energy of −57.5 kJ/mol. The Fe1−CO distance to be broken on the nonet surface is about 13% longer in **C4** than in **11_Sp**. The other bond distances, the Fe1−O1, Fe1−N1, and Fe1−N2 bonds, are also lengthened slightly upon going from **11_Sp** to **C4**, indicating a weaker Fe-ligand interaction in **C4.**

To shed light on the mechanism of this intersystem crossing process, we investigated the frontier molecular orbitals for **C4**, lowest unoccupied molecular orbital (LUMO) for the septet state and highest occupied molecular orbital (HOMO) for the nonet state, as shown in Figure 4. The LUMO of **11_Sp** and **C4_Sp** corresponds to the Fe2 $d_{xy}$ orbital having Fe2-ligand $\sigma$-antibonding character (Figure 4a). In **C4_Nn**, the same Fe2 $d_{xy}$ orbital is forced to be singly occupied and turns into the HOMO (Figure 4b), resulting in the weakening of the Fe2-ligand bonds. The CO dissociation on the nonet surface alleviates the antibonding interaction by changing the ligand environment of Fe1 from four- to three-coordinate, and thus acts as a driving force for the reaction.

There is added complexity in this septet to nonet transition. An additional septet state species **11a_Sp** of similar energy to **11_Sp** exists with the carbonyl coordinated to a tetrahedral iron rather than a planar iron atom. These are related by the transition structure **5TS_Sp** which is 17.5 kJ/mol higher in energy than the **11_Sp** species. The MECP to the nonet state **11_Nn** from this state, **C5**, is 34.1 kJ/mol above **11a_Sp**. The net result of these possible pathways and intersystem crossings is the

(27) (a) Andres, H.; Bominaar, E. L.; Smith, J. M.; Eckert, N. A.; Holland, P. L.; Münck, E. *J. Am. Chem. Soc.* **2002**, *124*, 3012. (b) Eckert, N. A.; Stoian, S.; Smith, J. M.; Bominaar, E. L.; Münck, E.; Holland, P. L. *J. Am. Chem. Soc.* **2005**, *127*, 9344.

loss of CO and the formation of the di-$\mu$-oxo bridged iron(II) complex **12_Nn**.

On the nonet surface the species **5_Nn** is converted to **11_Nn** via the **4TS_Nn** transition structure. Here the Fe2 approaches closer to O1 with a Fe2−O1 distance of 1.887 Å, the Fe2−O2 bond is nearly broken, and the C−O1 bond is lengthened by 0.463 Å. The calculations show that Fe1 in **11_Nn** formed from the transition structure **4TS_Nn** adopts a stable arrangement in which the CO ligand bound to the iron atom Fe-1 has a pseudo-tetrahedral arrangement of ligands. This species undergoes a near barrierless ligand dissociation to give **12_Nn.**

**1.3. Electron Arrangements in the Transformation of 1_Sp to 12_Nn.** A combination of the resonance structures **1_Spa** and **1_Spb** was proposed by Holland, Münck, and Bominaar to describe the electronic structure of $L^{tBu}Fe-N_2-FeL^{tBu}$ (Scheme 2).[12c,d] Experimental and computational studies are consistent with **1_Spb** containing two high spin iron(II) ions antiferromagnetically coupled to the $N_2^{2-}$ triplet state ion. Our NBO analysis for **1_Sp** supports this idea and shows that only the $\beta$ electrons of the Fe metal centers are involved in the $\pi$ bonding interaction with the $N_2$ $\pi^*$ orbitals (see Supporting Information).

**Scheme 2**

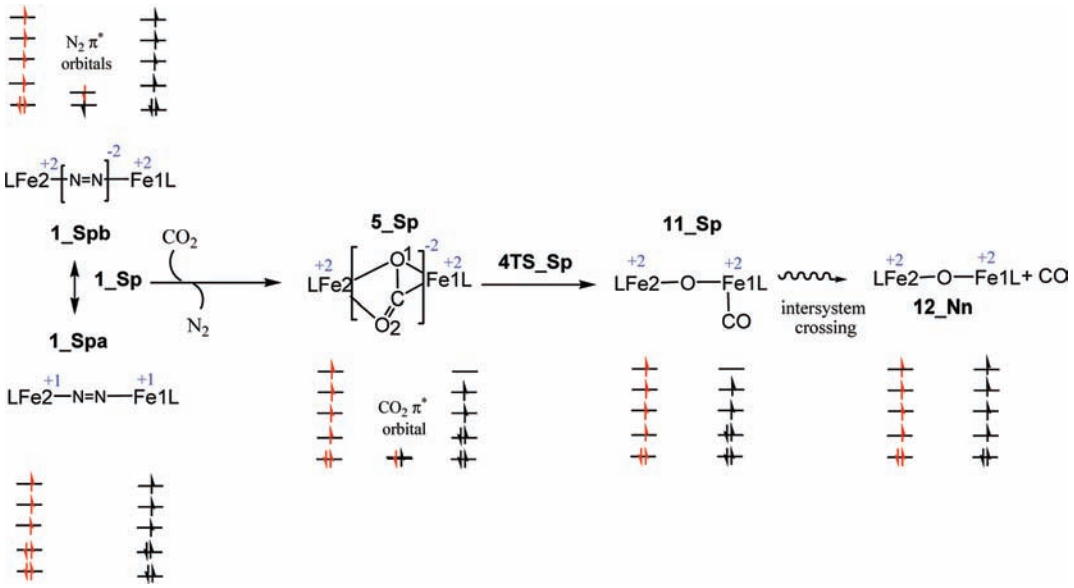


The reaction of $CO_2$ with **1_Sp** proceeds via a bridged transition structure to **3_Sp** followed by elimination of $N_2$ via the septet or nonet pathways. The $CO_2$ molecule becomes reduced in this sequence with electron density moving from the bridging dinitrogen. The initial reactants in an overall septet ($S$ = 3) state (LFe−$N_2$−FeL/$CO_2$) transform to the final nonet ($S$ = 4) state of the products (LFe($CO_3$)FeL/$N_2$/CO). This implies that at some point in the reaction path there will be a crossing from the septet to the nonet state. In the concerted reaction path **1_Sp** → **12_Nn** there are five identifiable MECPs, **C1** to **C5**. Two of these MECPs, **C1** and **C2**, lie well above low energy transition structures leading to the expectation that the reaction may kinetically follow the septet surface to **5_Sp**. The MECP point **C3** for the **5_Sp** → **5_Nn** crossing is low compared to the transition state energy for **4TS_Sp** (5.5 vs 29 kJ/mol). From the calculations in this work it is not possible to quantitatively predict the kinetic path as the spin forbidden reaction depends not only on the MECP energy but the surface hopping probability.[22,28] This probability is dependent on the spin orbit coupling between the septet and nonet states. What is clear is that the reaction **1-Sp** to **5-Sp** or **5_Nn** is thermodynamically favored.

Iron d electron population ($n_d$) analyses and electron spin densities ($\rho_s$) (B3LYP/BS3 model) of the iron atoms in **1_Sp** ($n_d$; $\rho_s$: 6.18; 3.69) correspond to the iron atoms in high spin Fe(II) ($S$ = 2) states. The septet state arises from antiferromagnetic coupling with a triplet state $N_2^{2-}$ species. Following $CO_2$ insertion and electron transfer from $N_2^{2-}$ to $CO_2$, to give **3_Sp**, the septet state arises from ferromagnetic coupling ($J$ = 68.2 $cm^{-1}$) of a high spin ($S$ = 2) Fe2(II) (6.30;3.60) with an intermediate spin ($S$ = 1) Fe1(II) (6.53;2.47). The corresponding **3_Nn** with $S$ = 0 is formed by antiferromagnetic coupling of two high spin Fe(II) ions, Fe1 (6.31;3.6) and Fe2 (6.35;3.54), $J$ = −22.8 $cm^{-1}$. This situation is followed for the septet and nonet surfaces with ferromagnetic coupling of $S$ = 2 and $S$ = 1 iron atoms for the septet states (**4_Sp** (6.54;2.07/6.32;3.57), 51.5 $cm^{-1}$; **5_Sp** (6.53;2.11/6.28;3.78), 1144 $cm^{-1}$; **11_Sp** (6.49;2.13/6.27;3.66), 1870 $cm^{-1}$; **11a_Sp** (6.42;2.09/6.28;3.69), 1019 $cm^{-1}$) and antiferromagnetic coupling for **4-Nn** with $S$ = 0 (6.31;3.58/6.34;3.55), −34.7 $cm^{-1}$; **5_Nn** with $S$ = 0 (6.27;3.58/6.27;3.67), −11.8 $cm^{-1}$; **12_Nn** with $S$ = 0 (6.29;3.56/6.29;3.56), −111.1 $cm^{-1}$; **13_Nn** with $S$ = 0 (6.29;3.63/6.27;3.67), −6.0 $cm^{-1}$.

To summarize this section, from the above analysis, the insertion of $CO_2$ between the two Fe atoms of LFe−$N_2$−FeL is the rate-determining step of the reductive cleavage reaction of $CO_2$. The moderate free energy

(28) (a) Zener, C. *Proc. R. Soc. London, Ser. A* **1932**, *137*, 696–702. (b) Nikitin, E. E. *Annu. Rev. Phys. Chem.* **1999**, *50*, 1–21. (c) Wittig, C. *J. Phys. Chem. B* **2005**, *109*, 8428–8430.

**Scheme 3**

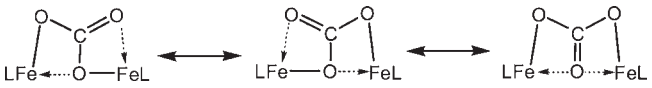

barrier calculated for the rate-determining step through either concerted or stepwise pathways agrees with the mild reaction conditions seen in experiment (the reaction was completed at room temperature after 18 h).[13] The intersystem crossing from septet to nonet forces the Fe1 $d_{xy}$ orbital to be occupied, resulting in the release of the CO ligand from Fe1 and the formation of LFeOFeL.[27]

**2.1. Formation of $LFeCO_3FeL$.** In LFeOFeL, similar to the experimental findings for $L^{tBu}Fe-O-FeL^{tBu}$,[27b] the Fe−O−Fe angle of 179.9° indicates a linear arrangement, and the two diketiminate planes with a dihedral angle of 77.0° are nearly perpendicular to each other. The linearity obtained for Fe−O−Fe in LFeOFeL can be explained in terms of the ionic behavior of the Fe−O−Fe bonding. The NBO analysis shows that the percentage contribution of oxygen to the Fe−O bonds in LFeOFeL is about 90%, implying ionic character to this bonding arrangement. The ionic character of the Fe−O bond most likely would reduce the tendency of the O atom to adopt an $sp^3$-hybridized orbital, resulting in a linear geometry for LFeOFeL.[27] In the literature, the linearity found in $L^{tBu}Fe-O-FeL^{tBu}$ was explained in terms of the $\pi$-bonding interaction between the oxygen lone pair electrons and the Fe centers.[12d] The NBO analysis shows that the oxygen $p_z$ lone pair $\beta$-electron density is slightly polarized toward the $p_z$ and $d_{yz}$ orbitals of one of the Fe centers (about 11.2%).

Beginning from **12_Nn**, $CO_2$ approaches the Fe-bound oxygen atom to yield carbonatodiiron(II) product **13_Nn** via a transition structure (**6TS_Nn**) lying 43.3 kJ/mol above **12_Nn**. The NBO analysis for **6TS_Nn** shows that one of the lone pairs on the oxygen bonded to the Fe centers interacts with one of the $\pi^*$ orbitals on $CO_2$, with a second order interaction energy of 82.4 kJ/mol. In **6TS_Nn**, the length of the C−O bond being formed is 2.141 Å (see Figure 2). The reaction between $CO_2$ and **12_Nn** is calculated to be 23.7 kJ/mol exergonic.[29] These results strongly support the experimental observations: Holland and co-workers reported that $L^{tBu}FeOFeL^{tBu}$ reacts rapidly with $CO_2$ at room temperature to yield $L^{tBu}FeCO_3FeL^{tBu}$.[13] We believe that the sufficiently long bond distances of Fe−O as well as the linearity of the Fe−O−Fe geometry, which together allow the simultaneous interaction of the oxygen atoms of $CO_2$ with the Fe centers, afford a rationale as to why the reaction **12_Nn** + $CO_2$ → **13_Nn** is energetically favorable. The short Fe1−O1 and Fe2−O2 bond distances of 2.041 Å in **13_Nn** support the notion that the O1 and O2 atoms strongly interact with the Fe centers, forming the thermodynamically stable carbonatodiiron complex. The Fe1−O3 and Fe2−O3 bond distances are elongated by 0.351 Å from 1.803 Å in **12_Nn** to 2.154 Å in **13_Nn**. The C−O1 and C−O2 bond distances in **13_Nn** are stretched up to 0.105 Å relative to those in the free $CO_2$ molecule (Figure 2). The C−O3 bond in **13_Nn** is about 0.080 Å shorter than the C−O single bond (1.419 Å) calculated for $CH_3OH$. Thus, the combination of Lewis structures shown in Scheme 3 appears to be the best description for the bonding in the carbonatodiiron(II) complex **13_Nn**.

**2.2. Two Alternative Pathways for Formation of $LFeCO_3FeL$.** Starting from **11_Sp**, there exist two other pathways, in addition to the one shown in Figure 3a, through which the formation of **13_Nn** might take place. The first step of these pathways is surmised to be the reaction on the septet surface, instead of the nonet surface, of $CO_2$ with **11_Sp** (Figure 3b). This reaction which passes through transition structure **6TS_Sp** produces **14_Sp** in an exergonic fashion. **14_Sp** has a square-pyramidal geometry with the O3 atom trans to the vacant site and the CO ligand occupying one of the basal sites. Because of the presence of one electron in the Fe $d_{z^2}$ orbital, the Fe−O3 bond is calculated to be longer than the Fe−O1 bond by 0.401 Å (Figure 3b). From **14_Sp** the reaction can split into two different pathways. One of them involves a spin state change from the septet state to the nonet state via the MECP **C6**. This process, which leads to the occupancy of the Fe1 $d_{xy}$ orbital, results in CO loss, producing the carbonatodiiron(II) product **13_Nn**. The results obtained from the location of the MECP, **C6**, show that the spin crossover barrier to the formation of **13_Nn** is approximately 21.7 kJ/mol above **14_Sp** (at the B3LYP/BS1 level, Figure 3b).

Another pathway corresponds to the rearrangement of **14_Sp** to the trigonal bipyramidal structure **15_Sp** and then to the square pyramidal structure **16_Sp** through the Berry pseudo-rotation mechanism. The computed relative energy surface for this Berry pseudo-rotation process is rather flat near the local minimum positions, making the location of the relevant transition structures difficult. The CO ligand in **16_Sp** coordinates to Fe on the apical position rather than the basal position. The calculated Fe−CO distance in **16_Sp** is much longer than that in **14_Sp** (about 0.520 Å, Figure 3b), indicating that the Fe−CO bond in **16_Sp** is weak enough to be dissociated. In **16_Sp**, the unpaired electron residing in the $d_{z^2}$ orbital prevents the CO ligand being strongly coordinated to Fe. The weakly bound CO ligand is easily expelled from the coordination sphere, giving the carbonatodiiron(II) complex $LFeCO_3FeL$ (**13_Sp**). $LFeCO_3FeL$ is unstable in the septet state and can undergo a spin crossover to become **13_Nn**. The MECP of the septet and nonet surfaces of $LFeCO_3FeL$ (**C7**) is located 13.6 kJ/mol above **13_Sp** (Figure 3b).

By comparing the energetics given in Figures 3a and b, one expects that the unimolecular intersystem crossing reaction **11_Sp** → **C4** → **12_Nn** with a barrier of 7 kJ/mol should be superior to the bimolecular reaction **11_Sp** + $CO_2$ → **14_Sp** with a barrier of 69.5 kJ/mol. Indeed, entropy makes the former more favorable than the latter. Thus, we conclude that of the various possible pathways we have studied, the most likely one is the spin change of **11_Sp** from the septet to the nonet state followed by the interaction of $CO_2$ with **12_Nn**.

**3. Formation of $LFe(CO)_2$.** As mentioned in the introduction, it is expected that the CO molecules released from

(29) It is here of interest to compare our mechanistic results with those obtained from Lin's study regarding the reduction of $CO_2$ to CO by a (NHC)Ni complex (ref 9). The study by Lin and co-workers is a slightly different situation as the nickel complex has to partially dissociate before the $CO_2$ can bind to the nickel(0) complex. In our case $CO_2$ binds to the starting complex in the concerted mechanism to give an −O=C− bridged species or in the stepwise mechanism to give an O bound complex. The bridged species is rather like **6** in the Lin paper except that the iron system still has the bridging $N_2$ which is the electron source for $CO_2$ reduction.

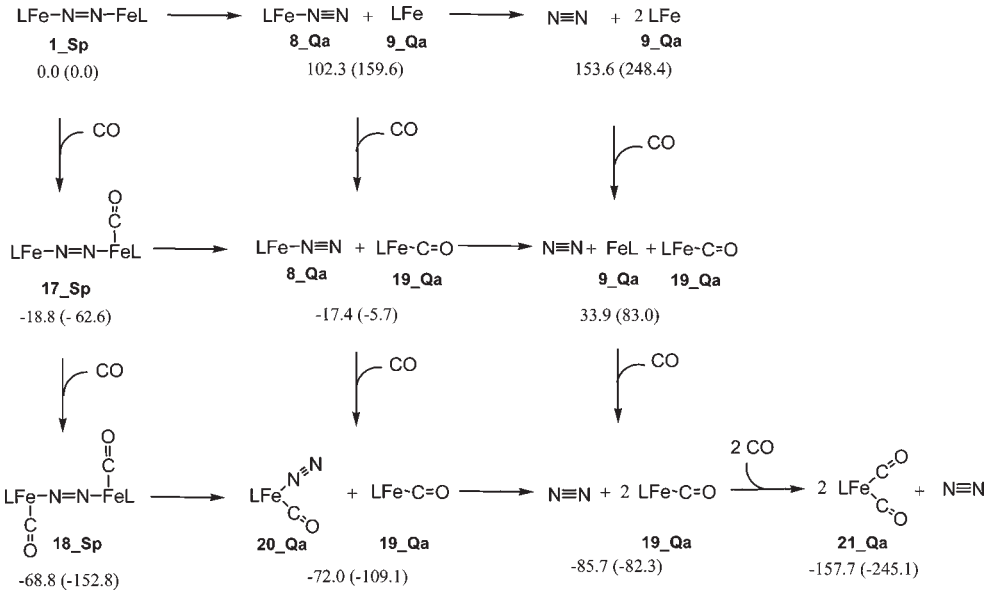


**Figure 5.** Different pathways leading to the formation of $LFe(CO)_2$ along with the calculated energetics of the expected intermediates. The relative free energies and electronic energies (in parentheses) obtained from the B3LYP/BS2//B3LYP/BS1 calculations are given in kJ/mol.

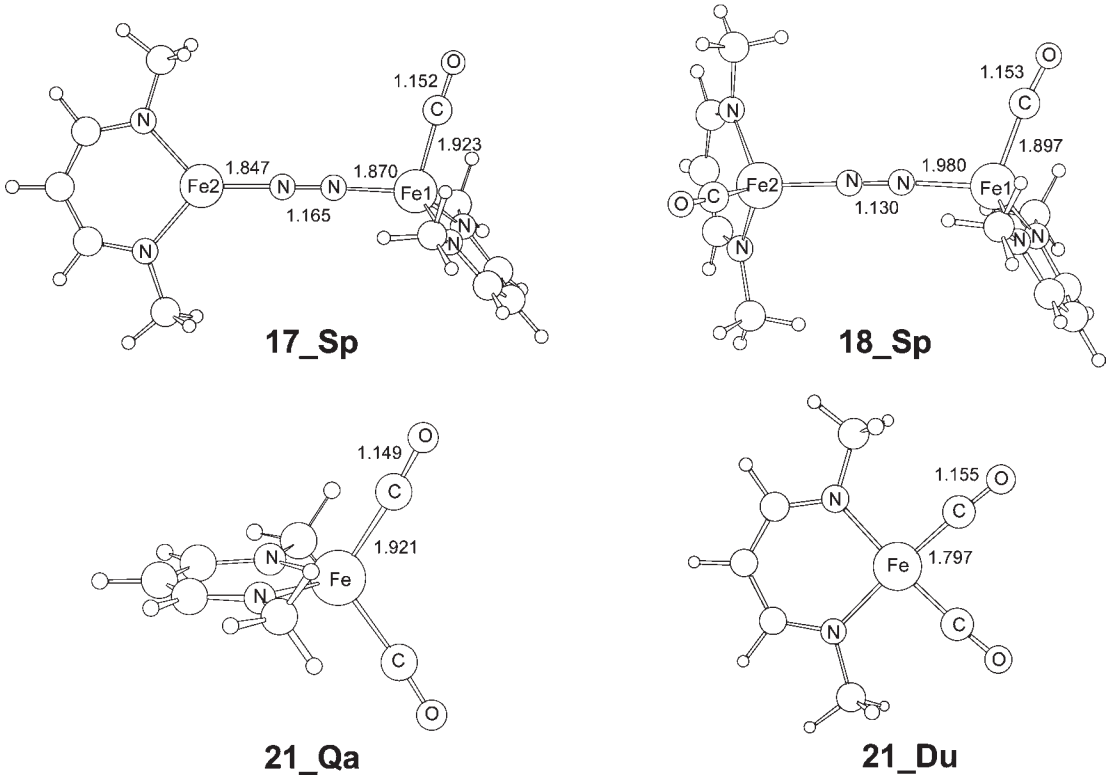


**Figure 6.** Optimized structures with selected structural parameters (bond lengths in Å) for some of the species shown in Figure 5.

the reaction **11_Sp** → **C4** → **12_Nn** + CO could interact with $LFeN_2FeL$ to afford $LFe(CO)_2$. To provide an overall picture of how $LFe(CO)_2$ is formed, the possible reaction pathways shown in Figure 5 were explored. From Figure 5, one may conclude that the pathway **1_Sp** → **17_Sp** → **18_Sp** → **20_Qa** + **19_Qa** → 2 (**19_Qa**) → 2 (**21_Qa**) is energetically the most favorable for the formation of $LFe(CO)_2$. The first steps involve consecutive coordination of one CO ligand to each Fe center forming **18_Sp**. This is followed by the dissociation of the two $Fe-N_2$ bonds and eventual coordination of another CO ligand to LFeCO (**19_Qa**) to generate $LFe(CO)_2$ (**20_Qa**). CO easily coordinates to Fe (without any barrier) at directions perpendicular to the diketiminate plane where the unfilled $p_z$ orbital of iron is available. The electron withdrawing ability of CO reduces the extent of the Fe-to-$N_2$ $\pi$-backbonding, weakening the $Fe-N_2-Fe$ bonds. The charge carried by $N_2$ is calculated to be −0.548, −0.449, and −0.208 for **1_Sp**, **17_Sp**, and **18_Sp**, respectively, suggesting that an increase in the number of the CO ligands

coordinated is accompanied by a decrease in the $\pi$-back-donating capability of the Fe centers. The Fe−$N_2$−Fe bonds in **17_Sp** are longer than in **1_Sp** and even longer in **18_Sp** (Figure 6) which indicates that the Fe−$N_2$ bond strength in these complexes decreases in the order **1_S*p*** > **17_S*p*** > **18_Sp**. This argument is reinforced by the calculated Fe−$N_2$ binding energies: 159.6 kJ/mol in **1_Sp**, 56.9 kJ/mol (the Fe1−$N_2$ bond) and 118.8 kJ/mol (the Fe2−$N_2$ bond) in **17_Sp**, and 43.7 kJ/mol in **18_Sp**.

The CO is coordinated to Fe more strongly in **18_Sp** than in **17_Sp**; the Fe−CO binding energy in **18_Sp** is calculated to be about 27.6 kJ/mol larger than in **17_Sp**. The Fe−CO bond distances in **18_Sp** are 0.026 Å shorter than that in **17_Sp**, and the calculated CO stretching modes shift to lower frequencies upon going from **17_Sp** (2075 $cm^{-1}$) to **18_Sp** (2059 and 2067 $cm^{-1}$). These results demonstrate that the presence of a carbonyl bound to one of the Fe centers of $LFeN_2FeL$ improves the $\pi$-back-donating capability of the other Fe center, resulting in the stronger Fe−CO bond in **18_Sp**.

It is also of interest to compare the Fe−CO bonding energies of **17_Sp** (62.6 kJ/mol), **11_Sp** (76.0 kJ/mol), and **11_Nn** (33.0 kJ/mol). CO interacts much more weakly with Fe in **11_Nn** than in **17_Sp**. This difference implies that the Fe center with a higher formal oxidation state, as in **11_Nn**, has a lower tendency to coordinate to CO because of Fe(II) being less susceptible toward $\pi$-back-bonding interactions when compared to Fe(I). On the other hand, the formal oxidation state of the Fe centers is +2 in both **11_Sp** and **11_Nn** yet they have very different CO binding energies. The optimized geometry around Fe1 in **11_Sp** is square planar (Figure 2) while in **11_Nn** it is tetrahedral. This indicates that the nonbonding $\sigma$ lone-pair type orbital of CO interacts with the Fe1 $d_{xy}$ orbital in **11_Sp** and with the $p_z$ and $d_{z^2}$ orbitals of Fe1 in **11_Nn.** The lack of an unpaired electron in the Fe1 $d_{xy}$ orbital of **11_Sp** gives a greater Fe−CO binding energy in **11_Sp** than in **11_Nn** which has an unpaired electron in the Fe1 $d_{z^2}$ orbital.

Once **21_Qa** has formed, the reaction ends with the formation of **21_Du**, after passing a MECP (**C8**) connecting the quartet and doublet surfaces. Consistent with the experimental observation,[12b,13] the calculations show that **21_Du** is about 11.1 kJ/mol lower in energy than **21_Qa**, and the spin crossover barrier to the formation of **21_Du** is approximately 34.7 kJ/mol (at the B3LYP/BS1 level). As opposed to the tetrahedral geometry of **21_Qa**, **21_Du** has a square planar geometry (Figure 6) because of the absence of iron electron(s) residing in $d_{xy}$. It is also worth noting that the presence of the two strong $\pi$-accepting ligands is required to bring a four coordinate Fe complex on the doublet surface below the quartet. For instance, the complex $LFe(CO)(N_2)$, with only one CO ligand, on the doublet surface is about 21.6 kJ/mol less stable than on the quartet surface.

For the sake of completeness, we also studied the CO insertion between the two Fe atoms starting from **17_Sp** as a competitive side reaction. The results show that the reaction **17_Sp** → LFeCOFeL + $N_2$ is not competitive with the reaction **17_Sp** + CO → **18_Sp** from an energetic point of view. The reaction **17_Sp** → LFeCOFeL + $N_2$ requires a free energy activation barrier of 79.4 kJ/mol and is endergonic by about 10.5 kJ/mol (see Supporting Information, Figure S3). Also, our calculations show that LFeCO-FeL is not stable and is converted to $LFe(CO)_2$ when an excess of CO exists (see Supporting Information, Figure S4).

## Conclusions

DFT has been used to analyze in detail the mechanism for the reductive cleavage of $CO_2$ by the diiron(I) complex $LFeN_2FeL$ (L = $HC(CHNMe)_2$). The results indicate that the reaction starts on the septet surface and occurs through $CO_2$ insertion between the two Fe atoms of LFe−$N_2$−FeL and then release of $N_2$, followed by the reductive cleavage of $CO_2$ to afford an LFeOFe(CO)L structure. The insertion of $CO_2$ between the two Fe atoms is the rate-determining step of the reductive cleavage reaction of $CO_2$. There are several possible paths leading to reductive cleavage involving either movement along the septet surface or via intersystem crossings to the nonet surface.

LFe2−O−Fe1(CO)L on the septet surface can undergo an intersystem crossing from septet to nonet, subsequently giving LFeOFeL + CO. The intersystem crossing from septet to nonet forces the Fe1 $d_{xy}$ orbital to be occupied, resulting in the release of the CO ligand from Fe1 and the formation of LFeOFeL. LFeOFeL readily reacts with $CO_2$ to give $LFeCO_3FeL$. The final section of this paper shows that CO released from the intersystem crossing process can easily interact with $LFeN_2FeL$ to afford $LFe(CO)_2$.

This work confirms the complexity of reaction mechanisms involving iron species and shows that one needs to consider multiple intersystem crossings and molecular interactions to obtain an accurate picture of the possible pathways for product formation.

**Acknowledgment.** We thank the Australian Research Council for funding, the National Computational Infrastructure (NCI), and the Tasmanian Partnership for Advanced Computing (TPAC) for provision of computing resources, and the University of Tasmania for hosting P.D.W.B. during his sabbatical visit.

**Supporting Information Available:** Further details are given in Scheme S1, Figures S1−S6, and Tables S1−S3. This material is available free of charge via the Internet at http://pubs.acs.org.